ARTICLE NO. 79-4108

Thick Axisymmetric Turbulent Boundary Layer on a Circular Cylinder

Nuray Denli* and Louis Landweber†
University of Iowa, Iowa City, Iowa

Two similarity laws for a thick, axisymmetric, turbulent boundary layer on a long circular cylinder are presented. In the law-of-the-wall region, the validity of the assumption of a constant-stress moment is analyzed and a new logarithmic mixing-length model, which takes into account the transverse-curvature effect on turbulence, is proposed. Using this mixing-length model, a law of the wall is derived which is given in terms of the exponential integral in the logarithmic portion. When the boundary layer is very thick relative to the radius of the cylinder, the flow in the outer region of the boundary layer is similar to an axisymmetric wake. With this analogy, a velocity-defect law is derived in terms of confluent hypergeometric functions known as Kummer functions. Both similarity laws are compared with the available data.

Nomenclature

a = radius of cylinder
a^* = frictional Reynolds number based on cylinder radius ($=au_\tau/\nu$)
l, l^* = dimensional and nondimensional mixing length, respectively ($l^*=lu_\tau/\nu$)
$\bar{r}$ = nondimensional radial distance ($=r/a$)
R = nondimensional boundary-layer thickness $=(\delta+a)/a$
Re_a = Reynolds number based on freestream velocity and cylinder radius ($=aU_e/\nu$)
R_x = Reynolds number based on freestream velocity and longitudinal coordinate x ($=xU_e/\nu$)
(u, v) = longitudinal and radial velocity components
$u_d, \bar{u}_d$ = dimensional and nondimensional velocity defect, respectively [$u_d=U_e-u$, $\bar{u}_d=(u_d/U_e)\sqrt{Re_a}$]
u^* = nondimensional velocity ($=u/u_\tau$)
u_τ = friction velocity ($=\sqrt{\tau_w/\rho}$)
U_e = freestream velocity
(x, r) = cylindrical coordinates
(x, y) = cylindrical coordinates ($y=r-a$)
y^* = nondimensional radial distance ($=yu_\tau/\nu$)
δ = boundary-layer thickness
δ^*, δ_1 = displacement thicknesses [$\delta_1=\delta^*(1+\delta/2a)$]
ϵ = eddy viscosity
θ, θ_1 = momentum thicknesses [$\theta_1=\theta(1+\theta/2a)$]
μ = dynamic viscosity of the fluid
ν = kinematic viscosity of the fluid
(ξ, η) = nondimensional longitudinal and radial coordinates, respectively [$\xi^2=(x/a)/Re_a$, $\eta=(y+a)/(\delta+a)$]
ρ = fluid density
σ, σ' = U_e/u_τ, $d\sigma/dR_x$, respectively
τ, τ^+, τ_w = total shear stress, nondimensional shear stress ($=\tau/\tau_w$), wall-shear stress

Received Feb. 22, 1979.

Index categories: Boundary Layers and Convective Heat Transfer—Turbulent.

*Post Doctorate Research Scientist, Iowa Institute of Hydraulic Research.

†Professor and Research Engineer, Iowa Institute of Hydraulic Research.

Introduction

FOR a turbulent boundary layer growing on a transversely curved surface, the flow has a different structure than for a flat-plate boundary layer if the boundary-layer thickness δ is of the same or higher order than that of a typical transverse dimension of the body. This difference is of importance in computation of the boundary layer near the tail of a body of revolution, in estimating the surface resistance of ship models, or other three-dimensional elongated bodies.

Since the pressure gradient is almost zero everywhere, and there is no strong interaction between the boundary layer and the external flow, the turbulent boundary layer on the circular cylinder is a special case of the problem of transverse-curvature effect. Because of the simple geometry which isolates the effect of transverse curvature from that of the longitudinal radius of curvature of other elongated axisymmetric bodies, this problem has been studied in the past both by experimental and theoretical methods. In 1949, Landweber[1] investigated the transverse-curvature effect by using the 1/7th power law and the Blasius skin-friction law. Qualitatively, he showed that the skin friction on the cylinder was greater than that of a flat plate corresponding to the same momentum-thickness Reynolds number. Most of the other investigations in this area were only concerned with the inner layer, particularly with the so-called logarithmic portion of the inner layer. Richmond,[2] Rao,[3] Yu[4] and Chin et al.,[5] all assumed that the classical two-dimensional law of the wall had to be modified. Richmond[2] and Rao[3] modified the argument of the logarithm and retained the constants of the two-dimensional logarithmic law. Later, however, Rao and Keshavan,[6] on the basis of their experimental data, proposed that the constants are "functions" of Re_a and a^* for axisymmetric flows. On the other hand, Yu[4] and Chin et al.[5] kept the form of the two-dimensional logarithmic law but tried to modify the constants depending on their experimental data. Other work done in this area employed closure models of two-dimensional turbulent flows in conjunction with the assumption of constant stress moment in the law-of-the-wall region. In this group, Sparrow et al.[7] used Deissler's eddy-viscosity model, and Patel[8] used a mixing length model given by Landweber and Poreh.[9]

Although the boundary layer on a long slender rod, when $\delta/a>>1$, is almost all a wake-like flow, very little attention has been paid to the outer portion of the boundary layer. Rao and Keshavan[6] tried to find a similarity variable for the velocity-defect region by trial and error. They found that the velocity defect $(U_e-u)/u_\tau$ yields similarity in terms of the variable $r^*=[(a+y)u_\tau]/\nu$. On the other hand, Yu[4] and

Chin et al.[5] presented their measurements in classical two-dimensional defect-law coordinates and tried to adjust the constants.

In 1972, White[10] approached the problem with a simple integral analysis in which he assumed that the law of the wall suggested by Rao[3] is valid throughout the boundary layer. Thus, the wake portion of the boundary layer was not considered.

In 1979, Cebeci[11] solved the turbulent boundary-layer equations by an implicit finite-difference method, applied after the momentum equations had been linearized. In this treatment, Cebeci used an eddy-viscosity model of thin, two-dimensional boundary layers which ignores the effect of transverse curvature on turbulence. However, Cebeci's solution is the only complete one available.

In 1976, Afzal and Narasimha[12] studied the problem at large values of the frictional Reynolds number based on the radius of cylinder a, $a^* = au_\tau/\nu$, with the boundary-layer thickness δ of order a. They used the equations of the mean flow and the method of matched asymptotic expansions to show that the flow can be described by the inner- and outer-layer concepts that are used in two-dimensional turbulent boundary layers.

Some of the researchers, however, performed only experimental work, namely: Yasuhara,[13] and Willmarth et al.[14,15] The only measurements of turbulent quantities (except the wall-pressure fluctuations measured by Willmarth et al.) are given by Afzal and Singh.[16]

Although a large number of measurements of the mean-velocity profiles are available, the similarity laws for the axisymmetric turbulent flow along a circular cylinder have not as yet been well established. In this paper, similarity will be derived by using the mean-flow momentum equation and closure relations for the Reynolds shear-stress distribution, and these will be applied to calculate boundary-layer characteristics.

The Law of the Wall

For a turbulent boundary layer on a circular cylinder, the mean-flow streamlines remain almost parallel to the surface; hence, the normal component of the mean velocity, v, is much smaller than the longitudinal component, u. Consequently, the induced pressure gradient is negligible. In terms of the cylindrical coordinates (x, r) and/or (x, y), the boundary-layer equations for the mean flow are

$$u\frac{\partial u}{\partial x} + v\frac{\partial u}{\partial y} - \frac{\partial}{\rho r \partial y}(r\tau) = 0 \tag{1}$$

$$\frac{\partial (ru)}{\partial x} + \frac{\partial (rv)}{\partial y} = 0 \tag{2}$$

where

(x, y) = coordinates parallel and perpendicular to the axis of symmetry of the cylinder, respectively.

u $= u(x, y)$, $v = v(x, y)$ are the mean-velocity components in the x and y directions.

r $= a + y$, with a the radius of the cylinder.

τ $= \tau(x, y)$ is the total shear stress, which is given by

$$\tau = \mu\frac{\partial u}{\partial y} - \rho\overline{u'v'} \tag{3}$$

Here ρ and μ are the density and the dynamic viscosity of the fluid, and $\rho\overline{u'v'}$ is the so-called Reynolds shear stress due to the fluctuating components u' and v' of the instantaneous velocity.

The boundary conditions are

$$u(x, 0) = 0, \qquad v(x, 0) = 0 \tag{4}$$

$$\lim_{y\to\infty} u(x,y) = U_e, \quad \lim_{y\to\infty} v(x, y) = 0 \tag{5}$$

where U_e is the velocity at the edge of the boundary layer.

Equations (1) and (2) can be solved if a closure relationship for the Reynolds shear stress is assumed.

The simplest and the most commonly used closure relations are given by the classical phenomenological theories, which relate Reynolds stresses to the mean flow through the well-known concepts of mixing length and eddy viscosity. Using the mixing-length concept, Patel[8] gives the velocity distribution in the law-of-the-wall region as

$$u^* = \int_0^{y^*} \frac{2\tau^+ \, dy^*}{1+\sqrt{1+4l^{*2}\tau^+}} \tag{6}$$

where

$$\tau^+ = \frac{\tau}{\tau_w}, \quad u^* = \frac{u}{u_\tau}, \quad y^* = \frac{u_\tau y}{\nu}, \quad l^* = \frac{u_\tau l}{\nu}, \quad u_\tau = \sqrt{\frac{\tau_w}{\rho}} \tag{7}$$

τ_w = the shear stress at $y = 0$, l = mixing length.

For thin boundary layers, there are numerous formulations for the mixing-length distribution. As discussed by Patel,[8] the most recent and appropriate one, given by Landweber and Poreh,[9] is

$$l^* = \kappa y^* \sqrt{\tanh(\lambda^2 y^{*2})} \tag{8}$$

where $\kappa = 0.418$ is the von Kármán constant, and $\lambda = \sqrt{3}/63$ is a constant given by Patel.[8]

For a flat-plate boundary layer, τ^+ is assumed to be unity and Eqs. (6 and 8) give the law of the wall. For an axisymmetric, turbulent boundary layer, however, it is well known that the total stress, τ, does not remain constant in the law-of-the-wall region, although, under certain conditions, the stress moment $(r\tau)$ can be assumed to be constant and equal to $(a\tau_w)$.

A. Analysis of Shear-Stress Distribution

Dimensional analysis, applied to the wall variables $(u, y, a, \tau_w, \rho, \nu)$, gives the functional relation

$$u^* = f(y^*, a^*) \tag{9}$$

As discussed by Patel,[8] relaminarization occurs for $a^* < 28$, and as discussed by Afzal and Narasimha,[12] transition may be present for $28 < a^* < 106$. Hence, we shall assume in the following equations that $a^* > 106$. Assuming the functional relation given by Eq. (9), Eqs. (1, 2 and 9) give an expression for τ^+ as follows:

$$\frac{\partial u}{\partial x} = \frac{\partial}{\partial x}[u_\tau f(y^*, a^*)] = \frac{du_\tau}{dx}\left[\frac{\partial (y^* f)}{\partial y^*} + \frac{a^* \partial f}{\partial a^*}\right]$$

The data of Willmarth et al.[15] show that the term $\partial f/\partial a^*$ is negligible in the previous expression, as has been verified analytically in the solution obtained for the law of the wall, presented in a subsequent section. Therefore, the above expression for $\partial u/\partial x$ can be approximated by

$$\frac{\partial u}{\partial x} = \frac{du_\tau}{dx}\frac{\partial (y^* f)}{\partial y^*} \tag{10}$$

$$\frac{\partial u}{\partial y} = \frac{u_\tau^2}{\nu}\frac{\partial f}{\partial y^*} \tag{11}$$

From Eqs. (2 and 10), one obtains, after integrating by parts,

$$v = -\frac{\nu}{u_\tau}\frac{du_\tau}{dx}\left[y^* f - \frac{l}{a^* + y^*}\int_0^{y^*} y^* f \, dy^*\right] \tag{12}$$

Then Eqs. (9, 10, 11, and 12) give, with $f' \equiv \partial f/\partial y^*$,

$$u\frac{\partial u}{\partial x} + v\frac{\partial u}{\partial y} = u_\tau \frac{du_\tau}{dx}\left[f^2 + \frac{f'}{a^*+y^*}\int_0^{y^*} y^* f dy^*\right] \quad (13)$$

Also, with $\tau = \tau_w \tau^+ = \rho u_\tau^2 \tau^+$, the right-hand side of Eq. (1) becomes

$$\frac{1}{\rho r}\frac{\partial}{\partial y}(r\tau) = \frac{u_\tau^3/\nu}{a^*+y^*}\frac{\partial}{\partial y^*}[(a^*+y^*)\tau^+] \quad (14)$$

Substitution of Eqs. (13 and 14) into Eq. (1) now gives

$$\frac{\partial}{\partial y^*}[(a^*+y^*)\tau^+] = -\sigma'\left[(a^*+y^*)f^2 + f'\int_0^{y^*} y^* f dy^*\right] \quad (15)$$

where

$$\sigma' = \frac{d\sigma}{dR_x}, \qquad \sigma = \frac{U_e}{u_\tau}, \qquad R_x = \frac{U_e x}{\nu}$$

After integration by parts, some simplification, and application of the boundary conditions $\tau^+(0, y) = 1$ and $f(0, a^*) = 0$, Eq. (15) becomes

$$\tau^+ = \frac{a^*}{a^*+y^*}\left\{1 - \sigma'\int_0^{y^*} f(\xi)\left[f(\xi) + \frac{f(y^*)}{a^*}\xi\right]d\xi\right\} \quad (16)$$

For small values of y^* and σ', such that the integrals in Eq. (16) are negligible, τ^+ can be approximated by

$$\tau^+ = \frac{a^*}{a^*+y^*} \quad (17)$$

On the other hand, if the inertia terms in Eq. (1) are neglected and the remaining equation is integrated with respect to y, the same expression for τ^+, given in Eq. (17), is obtained. Thus the integral term in Eq. (16),

$$c(y^*, a^*, \sigma') \equiv \sigma'\int_0^{y^*} f(\xi)\left[f(\xi) + \frac{f(y^*)}{a^*}\xi\right]d\xi \quad (18)$$

represents the effect of inertia on the distribution of the shear stress τ^+ across the boundary layer at a given section.

The shear-stress distribution given by Eq. (17) has been used widely in the literature. It assumes that the inertia terms in the boundary-layer equation are negligible, and hence that the stress moment, $r\tau$, is constant in the law-of-the-wall region, at a given section. The relative magnitude of the "inertia" term in Eq. (16) can be obtained from the Taylor-series expansion

$$r\tau = a\tau_w + y\left.\frac{\partial(r\tau)}{\partial y}\right|_{y=0} + \frac{y^2}{2}\left.\frac{\partial^2(r\tau)}{\partial y^2}\right|_{y=0} + \frac{y^3}{6}\left.\frac{\partial^3(r\tau)}{\partial y^3}\right|_{y=0^+} + \cdots \quad (19)$$

By applying the nonslip condition to Eqs. (1 and 2) and their derivatives, one finds

$$\left.\frac{\partial(r\tau)}{\partial y}\right|_{y=0} = \left.\frac{\partial^2(r\tau)}{\partial y^2}\right|_{y=0} = 0, \left.\frac{\partial^3(r\tau)}{\partial y^3}\right|_{y=0} = \frac{\rho a}{\mu^2}\tau_w\frac{d\tau_w}{dx} \quad (20)$$

and hence, in nondimensional form,

$$\tau^+ = \frac{a^*}{a^*+y^*}\left(1 - \frac{1}{3}\sigma' y^{*3} + \cdots\right) \quad (21)$$

A typical value of σ' for a flat-plate boundary layer[9] is $\sigma' = 6\times10^{-6}$. Therefore, at $y^* = 30$, $(\sigma'/3)y^{*3} = 0.054$, and hence, the error in using Eq. (17) for the shear-stress distribution would be of the order of 5.4%. Equations (19 and 21) indicate that, as y^* increases, the contribution from the inertia term $c(y^*, a^*, \sigma')$ would increase, although, according to their derivations,these equations are valid only near the wall.

B. Numerical Solution of the Law of the Wall

Under the assumption of similarity, Eq. (6), together with Eqs. (8 and 16), defines the law of the wall for the axisymmetric turbulent boundary layer. From these equations, a more exact evaluation of the importance of the inertia terms can be obtained as follows:

We write Eq. (6) in the form

$$\frac{\partial f}{\partial y^*} = \frac{2\tau^+}{1 + [1 + 4\kappa^2 y^{*2}\tanh(\lambda^2 y^{*2})\tau^+]^{1/2}} \quad (22)$$

For various values of a^* and σ', Eqs. (22 and 16) have been solved simultaneously by using the modified Adams-Bashforth method and Simpson's 1/3 rule, respectively. The distributions of the shear stress given by Eqs. (16 and 17) are shown in Fig. 1. The law-of-the-wall range increases as a^* increases. For the largest value of y^* where the law of the wall is valid, estimated from Willmarth's data, the contributions of the inertia terms to the shear-stress distribution for $\sigma' = 10^{-5}$ and for various values of a^* are shown in Table 1. Also, knowing that $c(y^*, a^*, \sigma')$ is much less than 1, and writing Eq. (16) in the form $\tau^+ = \tau_0^+(1-c)$, then from Eq. (6), one obtains

$$u^* \approx \int_0^{y^*} \frac{2\tau_0^+(1 - c/2)dy^*}{1 + \sqrt{1 + 4l^{*2}\tau_0^+}}, \qquad \tau_0^+ = \frac{a^*}{a^*+y^*}$$

This shows that the percentage error introduced by using τ_0^+, rather than $\tau^+ = \tau_0^+(1-c)$, is reduced by a factor of two in the nondimensional velocity distribution, u^*. Therefore, the effect of the inertia terms on the shear stress and, consequently, on the velocity distributions can be neglected if $\sigma' < 10^{-5}$, a result consistent with the assumed functional form, $u^* = f(y^*, a^*)$. Indeed, if the inertia terms were not negligible, the functional form for u^* would be $f(y^*, a^*, \sigma')$, where $\sigma' = \sigma'(R_x, a^*)$. Therefore, throughout the remainder of this study, the inertia terms will be neglected in the law-of-the-wall region, and the distribution of the shear stress will be approximated by Eq. (17).

C. Analysis of Mixing-Length Distribution

The mixing-length model,[9] $l^* = \kappa y^* \tanh(\lambda^2 y^{*2})$, gives the correct asymptotic behavior and is continuous throughout the law-of-the-wall range,[8] for thin boundary layers. However, in the case of a thick axisymmetric turbulent boundary layer developing on a cylinder of constant radius, experimental results[8,14,15,16] show that the mixing length is affected by the transverse curvature, and decreases markedly as the boundary-layer thickness increases relative to the local radius of curvature.

Table 1 Error due to inertia terms

a^*	y^*	$\tau_0^+ = a^*/(a^*+y^*)$	$\tau^+ = \tau_0^+(1-c)$	Correction to τ^+,%
50	169	0.2283	0.2265	0.794
100	244	0.2907	0.2872	1.203
500	444	0.5297	0.5196	1.893
1000	544	0.6477	0.6333	2.217

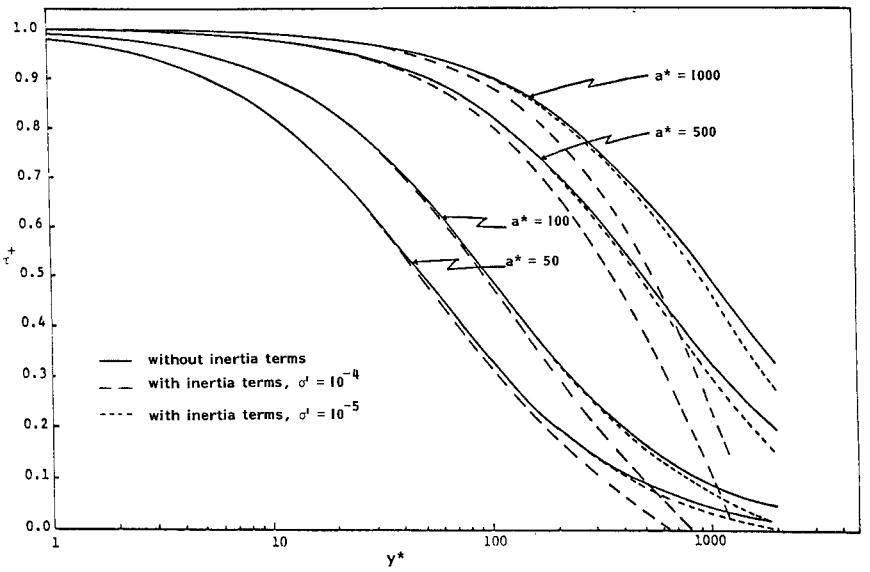

Fig. 1 Distribution of shear stress in law-of-the-wall region.

The mixing length is generally interpreted as the distance over which eddies transport momentum without losing their identity. Also, it is known that the large eddies contribute more to momentum transfer than small eddies. Hence, the mixing length, l, may be taken to be proportional to the dimension of the large eddies in the direction perpendicular to the main flow. Due to the geometry, the eddies on a circular cylinder can stretch more transversely, and hence are contracted in the direction perpendicular to the main flow, compared to the eddies of equivalent size on a flat plate. This argument suggests that the mixing length would be less on a circular cylinder than on a flat plate.

For a thin boundary layer, the sublayer relation is: $u^* = y^*$, and the mixing length in the fully turbulent region is: $l^* = \kappa y^*$. For an axisymmetric turbulent boundary layer, the sublayer relation is $u^* = a^* \ell n(1 + y^*/a^*)$. This suggests that, in the fully turbulent region, the mixing length should be replaced by

$$l^* = \kappa a^* \ell n(1 + y^*/a^*) \tag{23}$$

This assumption is reasonable because: 1) For a thick boundary layer, Eq. (23) yields smaller values of the mixing length than for a thin boundary layer, as required; 2) it has the correct asymptotic behavior, since

$$\lim_{a^* \to \infty} \kappa a^* \ell n(1 + y^*/a^*) = \kappa y^*$$

3) it is consistent with the relaminarization process observed in thick axisymmetric turbulent boundary layers, since we have

$$\lim_{a^* \to 0} a^* \ell n\left(1 + \frac{y^*}{a^*}\right) = 0$$

Consequently, for the axisymmetric turbulent boundary layer, Eq. (8) will be replaced by

$$l^* = \kappa a^* \ell n(1 + y^*/a^*) \sqrt{\tanh(\lambda^2 y^{*2})} \tag{24}$$

D. Analytical Solution in the Fully Turbulent Region

Once the distribution of the shear stress and the mixing length is established, the velocity distribution can be obtained from Eq. (6). Substitution of Eqs. (17 and 24) into Eq. (6) gives the velocity distribution as

$$u^* = \int_0^{y^*} \frac{2a^* dy^*}{(a^* + y^*)\left\{1 + \left[1 + 4\kappa^2 a^{*2} \ell n^2 (1 + y^*/a^*) \tanh(\lambda^2 y^{*2}) \frac{a^*}{a^* + y^*}\right]^{1/2}\right\}} \tag{25}$$

In the fully turbulent region, by order-of-magnitude considerations, Eq. (25) can be simplified and integrated analytically. In the fully turbulent region, $\tanh(\lambda^2 y^{*2})$ approaches unity and the term $4\kappa^2 a^{*2} \ell n^2(1 + y^*/a^*)[a^*/(a^* + y^*)]$ is much greater than 1. Hence, Eq. (25) may be reduced to

$$u^* = \int_{y_0^*}^{y^*} \frac{\sqrt{a^*}\, dy^*}{\sqrt{a^* + y^*}\, \kappa a^* \ell n(1 + y^*/a^*)} + B_r(a^*) \tag{26}$$

where $B_r(a^*)$ is the integral of Eq. (25) from zero to y_0^*, which is the value of y^* at which the viscous stresses become negligible in comparison with the Reynolds stresses. The change of variables, $z^2 = 1 + y^*/a^*$, transforms Eq. (26) to the well-known logarithmic integral[17] which may be expressed as the exponential integral,[17] $E_i(\ell n\, z)$, in the form

$$u^* = \frac{1}{\kappa} E_i[\ell n \sqrt{1 + y^*/a^*}] + B'(a^*) \tag{27}$$

where

$$B'(a^*) = \frac{-1}{\kappa} E_i[\ell n \sqrt{1 + y_0^*/a^*}] + B_r(a^*)$$

By introducing the infinite-series expansion of $E_i(x)$,[17] and the asymptotic condition that, as $a^* \to \infty$, $u^* \to (1/\kappa)\ell n y^* + B$, Eq. (27) can be written as

$$u^* = \frac{1}{\kappa} \ell n\left[a^* \ell n\left(1 + \frac{y^*}{a^*}\right)\right] + \frac{1}{\kappa} \sum_{n=1}^{\infty} \frac{[\ell n(1 + y^*/a^*)]^n}{2^n n \cdot n!} + B(a^*) \tag{28a}$$

where

$$B'(a^*) + \gamma = \frac{1}{\kappa} \ell n 2a^* + B(a^*) \tag{28b}$$

$\gamma = 0.5772156\ldots$ is the Euler constant.

Table 2 Comparison of relative magnitudes of terms in Eq. (28a)

a^*	y^*	y^*/a^*	1[a]	2[b]	3[c]	4[d]
198.2	227.4	1.147	5.020	0.3820	0.4219	0.73%
198.2	323.5	1.632	5.2565	0.4839	0.5493	1.13%
271.4	326.3	1.2023	5.3672	0.3948	0.4374	0.73%
1376.0	1981.0	1.4393	7.1123	0.4459	0.5009	0.72%

[a] $\ell n[a^* \ell n(1+y^*/a^*)]$. [b] $\frac{1}{2}\ell n(1+y^*/a^*)$ (first term of series). [c] $\sum_{n=1}^{5} \frac{[\ell n(1+y^*)/a^*]^n}{2^n n \cdot n!}$. [d] Percent error due to neglecting the infinite series after the first term.

The infinite series in Eq. (28) converges very rapidly. In fact, most of the contribution from the series comes from the first term. Table 2 shows the contribution of the infinite series for some typical values of y^* taken from Willmarth's data.[15]

Equation (25) has been integrated for various values of λ and compared with Willmarth's data.[15] The results are in good agreement for Patel's value,[8] $\lambda = \sqrt{3}/63$. With this value of λ, Eq. (25) gives the complete velocity distribution in the law-of-the-wall region. Hence, using the results from Eq. (25), the value of $B(a^*)$ can be calculated directly from Eq. (28). The variation of $B(a^*)$ with respect to $1/a^*$ is found to be linear, in agreement with Afzal and Singh,[16] and given by

$$B(a^*) = -\frac{41.76}{a^*} + 5.45 \tag{29}$$

Also, as shown in Table 2, the main contribution of the infinite series comes from the first term. A sufficiently accurate approximation to Eq. (28) is then given by

$$u^* = \frac{1}{\kappa}\ell n\left[a^*\sqrt{1+\frac{y^*}{a^*}}\,\ell n\left(1+\frac{y^*}{a^*}\right)\right] - \frac{41.76}{a^*} + 5.45 \tag{30}$$

For $y^*/a^* < 1$, the argument of the logarithm can be expanded as

$$Y^* \equiv a^*\sqrt{1+\frac{y^*}{a^*}}\,\ell n\left(1+\frac{y^*}{a^*}\right) \approx y^*\left[1 - \frac{1}{24}\left(\frac{y^*}{a^*}\right)^2 + \frac{1}{24}\left(\frac{y^*}{a^*}\right)^3 + \ldots\right] \tag{31}$$

Thus the argument of the logarithm, Y^*, behaves very nearly like y^*, even in the neighborhood of $y^*/a^* = 1$.

We can now verify the assumption that $\partial f/\partial a^*$ may be neglected, used in the derivation of Eq. (10), since

$$a^*\frac{\partial u^*}{\partial a^*} = a^*\frac{\partial f(y^*, a^*)}{a^*} \approx \frac{41.76}{a^*}$$

and, in the logarithmic range,

$$\frac{\partial}{\partial y^*}(fy^*) > f(y^*) > 10 > > \frac{41.76}{a^*} \quad \text{for} \quad a^* > 106$$

as required that the boundary layer be turbulent.

The data of Willmarth et al.[15] are compared with Eq. (25) and with the solution of Patel[8] in Figs. 2-4. A comparison of Eq. (25) with (30) is also shown in Fig. 2. As can be seen from this figure, the analytical approximation to Eq. (25), i.e. Eq. (30), is in excellent agreement in the range of the logarithmic portion of the law of the wall. In Fig. 5, the data of Willmarth et al.[15] are compared with Eq. (30) for various values of a^* and δ/a.

It is interesting to note that, if the infinite series is neglected, Eq. (28) is very similar to the logarithmic law proposed by Rao[3] from purely heuristic considerations. Rao obtained this logarithmic law simply by replacing y^* in the classical two-dimensional logarithmic law by the axisymmetric sublayer relation $a^*\ell n(1+y^*/a^*)$, and, initially, retaining the constants of the two-dimensional logarithmic law. Later, however, in 1972, based on their experimental data, Rao and Keshavan[6] proposed that the universal constants of the flat-plate boundary layer be replaced by functions of Re_a and a^* for axisymmetric flows. However, their wall shear-stress measurements are believed to be in error.[8]

It is important to emphasize that the argument y^* given by Eq. (31) behaves very nearly like y^* in the neighborhood of $y^*/a^* = 1$. This explains why the Preston-tube technique with the usual calibration curve gives good measurements of the wall-shear stress, and why some of the previous researchers, like Yu[4] and Chin et al.,[5] whose data are limited to $\delta/a < 2$, were able to retain the form of the classical two-dimensional logarithmic law.

The Velocity-Defect Law

The equations of the mean flow, u, and the boundary conditions for an axisymmetric wake are exactly the same as the mean-flow equations of a boundary layer growing on a cylinder of constant radius, except for the inner boundary condition. A thick, axisymmetric boundary layer is attained on an infinitely long cylinder when the radius of the cylinder is very small relative to the distance x from the nose. If the boundary-layer thickness relative to the transverse radius of curvature is large, the cylinder may be considered as a small vorticity- and turbulence-producing disturbance. Consequently, the flow might be considered similar to a wake flow with the modified inner boundary condition. The important difference is that the drag generating the wake is a function of the longitudinal coordinate in the present problem. With these considerations, the velocity-defect law has been derived in a manner similar to that which has been used for the axisymmetric turbulent wake, under the three assumptions that 1) $v \ll u$, 2) $\partial u/\partial r$ is small, and 3) the curvature of the mean-flow streamlines is negligible. Oseen's approximation is applicable. Under these assumptions, the mean-flow equation takes the form

$$U_e\frac{\partial u_d}{\partial x} = -\frac{1}{\rho r}\frac{\partial}{\partial r}(r\tau) \tag{32}$$

where $u_d = U_e - u$ satisfies the boundary condition

$$\lim_{r\to\infty} u_d(x,r) = 0$$

In terms of the nondimensional quantities

$$\xi^2 = \frac{x}{aRe_a}, \quad \tilde{u}_d = \frac{u_d\sqrt{Re_a}}{U_e}, \quad R = \frac{\delta + a}{a}$$

$$\tau^+ = \frac{\tau}{\rho u_\tau^2}, \quad \bar{r} = \frac{r}{a}, \quad \beta^2 = \frac{\sigma^2}{2Re_a^{3/2}}, \quad \sigma = \frac{Ue}{u_\tau} \tag{33}$$

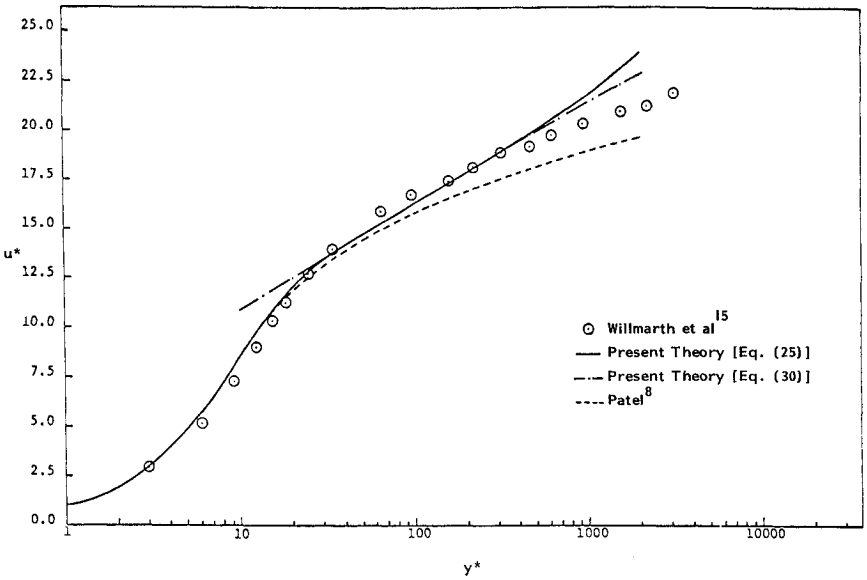

Fig. 2 Law of the wall for $\delta/a = 16$, $a^* = 198.2$.

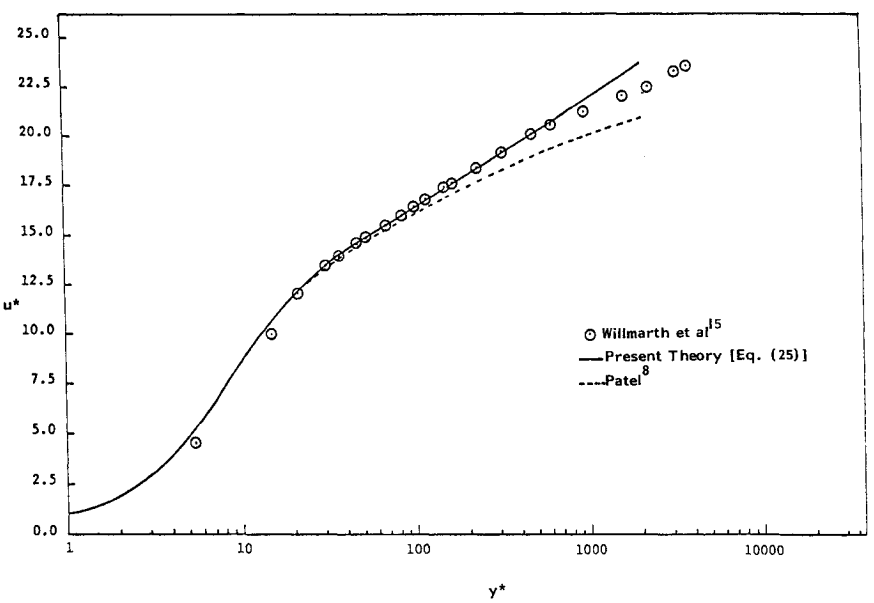

Fig. 3 Law of the wall for $\delta/a = 9.45$, $a^* = 398.2$.

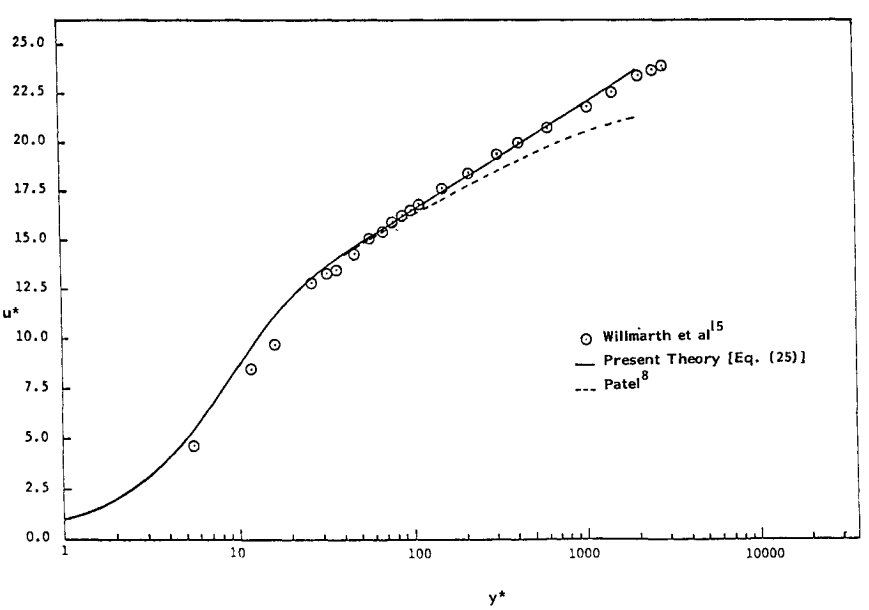

Fig. 4 Law of the wall for $\delta/a = 5.52$, $a^* = 531$.

suggested by the laminar boundary-layer solution of Glauert and Lighthill,[18] Eq. (32) becomes

$$\frac{\beta^2}{\xi}\frac{\partial \bar{u}_d}{\partial \xi} = -\frac{1}{\bar{r}}\frac{\partial}{\partial \bar{r}}(\bar{r}\tau^+) \tag{34}$$

E. Similarity Solution

If the velocity variation across the boundary layer in the velocity-defect zone is small compared with the freestream velocity, then the flow may be self-preserving. This suggests that the nondimensional velocity defect $\bar{u}_d$ may be of the separable form

$$\bar{u}_d = \chi(\xi) f(\eta), \qquad \eta = \frac{r}{\delta + a} = \frac{\bar{r}}{R} \tag{35}$$

The boundary conditions at $\eta = 1$ are

$$\bar{u}_d = 0, \qquad \tau^+ = 0 \tag{36}$$

Then we have

$$\frac{\partial \bar{u}_d}{\partial \xi} = \dot{\chi} f(\eta) + \chi \frac{\mathrm{d}f}{\mathrm{d}\eta}\frac{\mathrm{d}\eta}{\mathrm{d}R}\frac{\mathrm{d}R}{\mathrm{d}\xi} = \dot{\chi} f(\eta) - \frac{\chi \dot{R}}{R}\eta f' \tag{37}$$

where

$$\dot{\chi}(\xi) = \mathrm{d}\chi/\mathrm{d}\xi, \qquad \dot{R} = \mathrm{d}R/\mathrm{d}\xi, \qquad f' = \mathrm{d}f/\mathrm{d}\eta$$

and substitution of Eqs. (35 and 37) into Eq. (34) gives

$$\frac{\beta^2 R}{\xi}\left(\dot{\chi} f - \frac{\chi \dot{R}}{R}\eta f'\right) = -\frac{1}{\eta}\frac{\partial}{\partial \eta}(\eta \tau^+) \tag{38}$$

Integrating Eq. (38) with respect to η from η to 1, and using the boundary conditions given by Eq. (36) yields, after some manipulation,

$$\frac{\beta^2 \dot{R}\chi}{\xi}\left[\eta^2 f + \left(2 + \frac{R\dot{\chi}}{\dot{R}\chi}\right)\int_\eta^1 \eta f \mathrm{d}\eta\right] = \eta \tau^+ \tag{39}$$

Equation (39) is the basic equation for the velocity-defect law. In order to solve it, the variation of the shear stress needs to be assumed. Depending on the modeling of the shear stress, Eq. (39) gives different differential equations for $\chi(\xi)$ and $f(\eta)$.[19]

In general, for free turbulent flows such as jets and wakes, an eddy-viscosity assumption gives good results. Since flow in the velocity-defect region might be considered as a wake flow, the eddy viscosity will be assumed to be a function of the longitudinal coordinate, ξ, only. The distribution of the shear stress in terms of eddy viscosity, $\epsilon(\xi)$, is then given by

$$\tau = \rho\epsilon\frac{\partial u}{\partial r} = -\rho\epsilon\frac{\partial u_d}{\partial r} \tag{40}$$

Substitution of the nondimensional quantities given in Eq. (33) and the velocity defect given by Eq. (35) into Eq. (40) gives

$$\tau^+ = -\epsilon\frac{U_e}{u_\tau^2\sqrt{Re_a}}\frac{\chi}{aR}f' = -\frac{2\epsilon}{\nu}\beta^2\frac{\chi}{R}f' \tag{41}$$

Substituting Eq. (41) into Eq. (39) and rearranging gives

$$-\frac{1}{\eta f'}\left\{\eta^2 f + \left(2 + \frac{R\dot{\chi}}{\dot{R}\chi}\right)\int_\eta^1 \eta f \mathrm{d}\eta\right\} = 2\frac{\epsilon(\xi)}{\nu}\frac{\xi}{\dot{R}R} \tag{42}$$

The similarity assumption requires that

$$2 + \frac{R\dot{\chi}}{\dot{R}\chi} = 2b, \qquad a \text{ constant} \tag{43}$$

and

$$2\frac{\epsilon(\xi)}{\nu}\frac{\xi}{R\dot{R}} = \alpha^2, \qquad a \text{ constant} \tag{44}$$

The solution of Eq. (43), obtained by the method of separation of variables, is

$$\chi(\xi) = CR^{2(b-1)} \tag{45}$$

where C is a constant of integration.

In order to solve Eq. (44), it is necessary to know the function $\epsilon(\xi)$. For an axisymmetric turbulent wake, ϵ/ν is proportional to the longitudinal coordinate x with a power law as $x^{-1/3}$. Since it has been suggested that the flow in the velocity-defect region is analogous to axisymmetric wake flow, ϵ/ν may be assumed to be of the form

$$\frac{\epsilon(\xi)}{\nu} = D\xi^{m-1} \tag{46}$$

where m and D are constants. Hence, after substituting Eq. (46), the solution of Eq. (44) gives the boundary-layer thickness as

$$R = A\left(\frac{x/a}{Re_a}\right)^{(m+1)/4}\left[1 + \frac{K}{R^2}\right]^{-1/2} \qquad A = \frac{2}{\alpha}\sqrt{\frac{D}{m+1}} \tag{47}$$

where K is a constant of integration. Then Eq. (45) becomes

$$\chi = B\left(\frac{x/a}{Re_a}\right)^{[(m+1)/2](b-1)}\left(1 + \frac{K}{r^2}\right)^{(1-b)} \tag{48}$$

where $B = CA^{2(b-1)}$.

From Eq. (42), the equation for $f(\eta)$ is

$$\eta^2 f + 2b\int_\eta^1 \eta f \mathrm{d}\eta + \alpha^2 \eta f' = 0 \tag{49}$$

Differentiation of Eq. (49) with respect to η gives

$$\alpha^2 \eta f'' + (\alpha^2 + \eta^2) f' + 2(1-b)\eta f = 0 \tag{50}$$

The change of variables $\eta = \alpha\zeta$ eliminates α^2 in Eq. (50), which then reduces to

$$f''(\zeta) + \left(\zeta + \frac{1}{\zeta}\right)f'(\zeta) + 2(1-b)f(\zeta) = 0 \tag{51}$$

This satisfies the boundary conditions

$$\lim_{\zeta \to \infty} f(\zeta) = f'(\zeta) = 0 \tag{52}$$

The differential Eq. (51) has singular points at $\zeta = 0$ and $\zeta = \infty$. Since $\zeta = 0$ is a regular singular point, Eq. (51) has at least one nontrivial solution of the form

$$f(\zeta) = \zeta^s \sum_{k=0}^{\infty} a_k \zeta^k \tag{53}$$

Since $\zeta = \infty$ is an irregular singular point, a nontrivial regular solution may or may not exist in the neighborhood of $\zeta = \infty$.

On the other hand, the exact solutions of Eq. (51) can easily be obtained for the values of $b = 0, \frac{1}{2}, 1$.

Case 1: $b=0$

$$f(\zeta)=e^{-\zeta^2/2}\left(C_1\int\frac{e^{\zeta^2/2}}{\zeta}\,d\zeta+C_2\right) \tag{54}$$

This solution with $C_1=0$ corresponds to the wake-flow solution.

Case 2: $b=1/2$

$$f(\zeta)=e^{-\zeta^2/4}\left[C_1I_0\left(\frac{\zeta^2}{4}\right)+C_2K_0\left(\frac{\zeta^2}{4}\right)\right] \tag{55}$$

where $I_0(\zeta^2/4)$ and $K_0(\zeta^2/4)$ are the modified Bessel functions of the order zero of the first and second kinds, respectively.

Case 3: $b=1$

$$f(\zeta)=C_1\int\frac{e^{-\zeta^2/2}}{\zeta}d\zeta+C_2 \tag{56}$$

This case is impossible according to Eq. (45), since the velocity defect $\bar{u}_d$ decreases and $R(\xi)$ increases with increasing values of ξ; i.e., b must be less than 1.

The exact solutions of the differential equation for $b=0$, $1/2$, 1 suggest the form of $f(\zeta)$ to be

$$f(\zeta)=e^{-z}F(z), \qquad z=\zeta^2/2 \tag{57}$$

Substitution of Eq. (57) into Eq. (51) gives

$$zF''(z)+(1-z)F'(z)-bF(z)=0 \tag{58}$$

a confluent hypergeometric differential equation, particularly known as the Kummer equation. It has a regular singularity at $z=0$, and an irregular singularity at $z=\infty$. The method of Fröbenius gives only one linearly independent solution. Two linearly independent solutions are given by Abramowitz and Stegun[17] as

$$F_1(z)=M(b,1,z)=\sum_{n=0}^{\infty}\frac{(b)_n}{(n!)^2}z^n \tag{59}$$

$$F_2(z)=U(b,1,z)=-\frac{1}{\Gamma(b)}\left\{M(b,1,z)\,\ell n\,z+\sum_{n=0}^{\infty}\frac{(b)_n z^n}{(n!)^2}\times[\psi(b+n)-2\psi(1+n)]\right\} \tag{60}$$

where $M(b,1,z)$ is the Kummer function.

$$(b)_n=b(b+1)(b+2)\ldots(b+n-1), \qquad (b)_0=1$$

Here $\psi(b+n)$ is the logarithmic derivative of the gamma function $\Gamma(b+n)$, which is known as the Digamma (psi) function, and given as

$$\psi(b+n)=\frac{1}{(n-1)+b}+\frac{1}{(n-2)+b}+\ldots+\frac{1}{2+b}+\frac{1}{1+b}+\frac{1}{b}+\psi(b) \tag{61}$$

Here $\psi(b)=(d/db)[\ell n\Gamma(b)]$ is tabulated in Abramowitz and Stegun.[17] The infinite series in Eqs. (59 and 60) converge for all values of z. Therefore, the general solution for $f(\eta)$ is

$$f(\eta)=e^{-z}F(z)[C_1M(b,1,z)+C_2U(b,1,z)] \tag{62}$$

In the neighborhood of $z=\infty$, the functions $M(b,1,z)$ and $U(b,1,z)$ have simple asymptotic expansions.[17] For $z\to\infty$,

$$M(b,1,z)\approx\frac{1}{\Gamma(b)}e^z z^{b-1}[1+0(|z|^{-1})] \tag{63}$$

$$U(b,1,z)\approx z^{-b}[1+0(|z|^{-1})] \tag{64}$$

Hence, as $z\to\infty$ ($\eta\to\infty$), $f(\eta)$ becomes, asymptotically,

$$f(\eta)\approx C_1\frac{z^{b-1}}{\Gamma(b)}+C_2e^{-z}z^{-b}+0(|z|^{-1}) \tag{65}$$

In the outer region of the bounday layer, it is assumed that the mean flow behaves like an axisymmetric wake, for which the solution with the eddy-viscosity assumption gives the defect-velocity profiles in terms of an exponential function. Hence, if the boundary layer behaves like an axisymmetric wake in the velocity-defect region, the constant C_1 must be zero. Hence, the solution for $f(\eta)$ is

$$f(\eta)=e^{-z}U(b,1,z), \qquad z=\eta^2/(2\alpha^2) \tag{66}$$

and, from Eqs. (36, 45, and 66), the velocity defect is

$$\bar{u}_d=CR^{2(b-1)}e^{-z}U(b,1,z) \tag{67}$$

Here b, C, and α are constants to be determined from the experimental data. We have alaready seen that $b<1$. The following analysis indicates that b must be positive.

Since the flow area due to an increment Δr increases with the radial distance r, the major contribution to the displacement thickness comes from the velocity-defect region. The nondimensional displacement thickness can then be approximated by

$$\frac{\delta_1}{a}=\int_{\bar{r}_0}^{R}\frac{u_d}{U_e}\bar{r}\,d\bar{r} \tag{68}$$

where $\bar{r}_0$ is the point where the velocity-defect law begins to be valid. From Eq. (67) and the relation $z=r^{-2}/(2R^2\alpha^2)$, Eq. (68) becomes

$$\frac{\delta_1}{a}\approx\alpha^2CR^{2b}\int_{z_0}^{1/2\alpha^2}e^{-z}U(b,1,z)\,dz, \qquad z_0=\bar{r}_0^2/(2R^2\alpha^2) \tag{69}$$

Since the displacement thickness δ_1 increases with the boundary layer thickness δ, b must be a positive number. Thus we have $0<b<1$.

F. Determination of Constants and Numerical Evaluation

The Kummer function $U(b,1,z)$ was calculated from the infinite series in Eqs. (59 and 60). The error R_N due to truncation at $n=N$ is given by[19]

$$|R_N|<\frac{1}{\Gamma(b)}\frac{z^N\ell n[(N+1)/z]}{(N-1)!(1-z/N)}$$

for $z=5$, $N=25$, $|R_N|<10^{-6}/\Gamma(b)$. Therefore, the series may be truncated at $n=25$ for $z\le5$. For larger values of z, the asymptotic expansion of the Kummer function $U(b,1,z)$ should be used.[17]

Equations (47 and 67) contain six undetermined constants, namely: A, m, K, b, C, and α. These constants have been determined from the data of Willmarth et al.[15] and Keshavan.[6] In Eq. (47), as ξ goes to zero, R goes asymptotically to 1. Hence, we must have $K=0(1)$. Consequently, for large values of R, the factor $[1+(K/R^2)]^{-1/2}$ in Eq. (47) is negligible. The plot of $\xi^2=(x/a)/Re_a$ vs $R=(\delta+a)/a$ on log-log paper, for large values of R, then gave the value of m

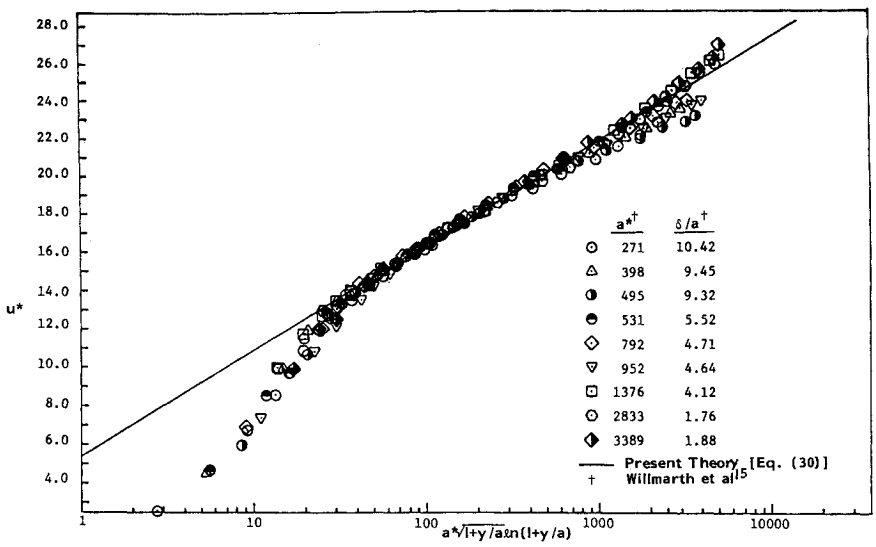

Fig. 5 Logarithmic portion of law of the wall.

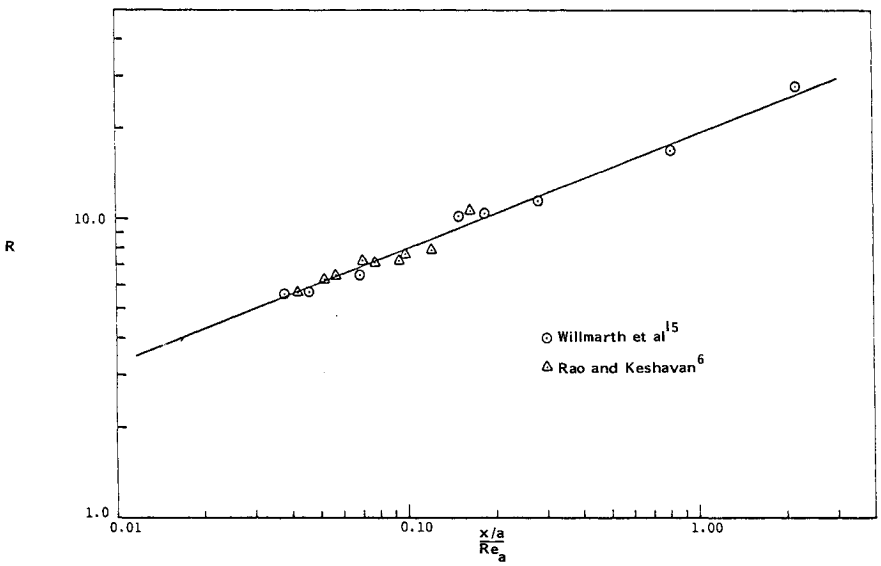

Fig. 6 Determination of value of m in Eq. (47).

as 7/13, from the slope of the best straight line drawn through the data, as shown in Fig. 6. Once the value of m had been obtained, the values of K and A were evaluated according to Eq. (47), by using all the available data. The values found were $A = 18.5$ and $K = -2$.

The values of b, α, and C (or B) were determined solely from the data of Willmarth et al.[15] Let

$$S = S(z) = Ce^{-z}U(b,1,z)$$

$$Y = \bar{u}_d = \left(1 - \frac{u}{U_e}\right)\sqrt{Re_a}$$

Then, according to Eq. (67),

$$Y = S(z)R^{2(b-1)} \tag{70}$$

Therefore, for each assigned value of z, $z = z_i$, the graph of Y vs R on log-log paper should give a straight line of slope $2(b-1)$ and intercept $S(z_i)$. Willmarth's data were plotted according to Eq. (70) for various constant values of z (or η), as shown in Fig. 7. The value of b, determined from the slope, was $b = 0.35$. Therefore, from Eq. (48), $\chi(\xi)$ becomes

$$\chi = B\sqrt{\frac{a}{x}}\sqrt{Re_a}\left(1 - \frac{2}{R^2}\right)^{0.65} \tag{71}$$

Hence, from Eqs. (35 and 67), the velocity defect becomes

$$\frac{U_e - u}{U_e} = B\sqrt{\frac{a}{x}}\left(1 - \frac{2}{r^2}\right)^{0.65} e^{-z}U(b,1,z), \quad z = \frac{\eta^2}{2\alpha^2} \tag{72}$$

Let

$$Z = \sqrt{\frac{x}{a}}\,\frac{U_e - u}{U_e}\left(1 - \frac{2}{R^2}\right)^{-0.65} \tag{73}$$

and

$$T = e^{-z}U(b,1,z), \quad b = 0.35, \quad z = \frac{\eta^2}{2\alpha^2} \tag{74}$$

After applying Eqs. (73 and 74), Eq. (72) becomes

$$Z = BT \tag{75}$$

The values of Z were obtained from Willmarth's data. The values of T, corresponding to the same values of η, were calculated from Eq. (74) for a range of values of α. The value of α which gave the best straight line passing through the origin was chosen. Consequently, the slope of the best straight

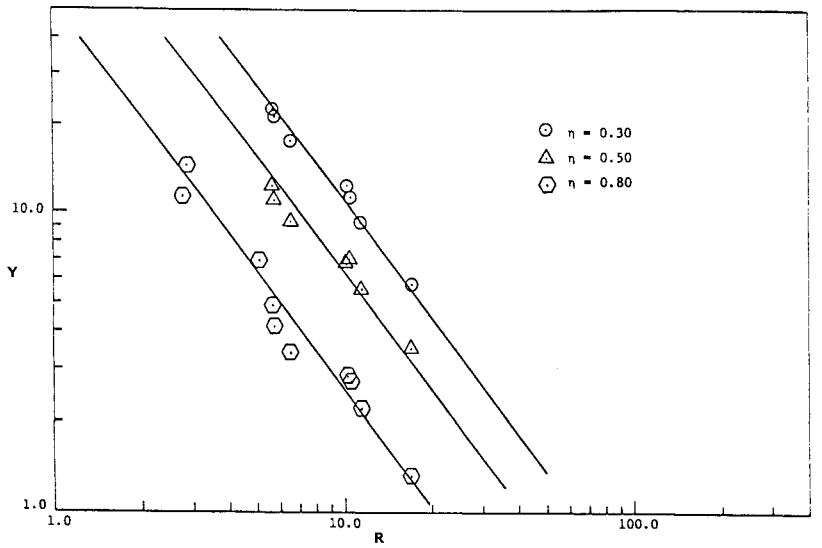

Fig. 7 Determination of value of b.

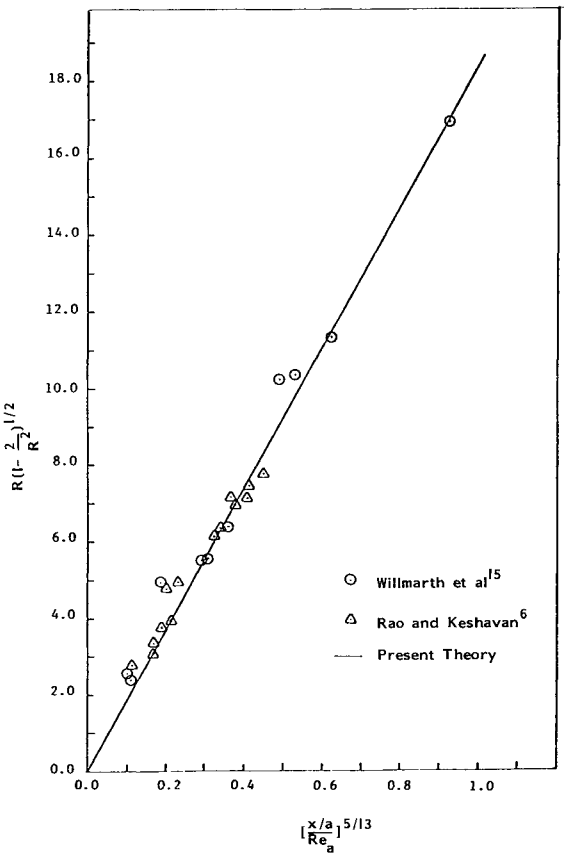

Fig. 8 Boundary-layer thickness.

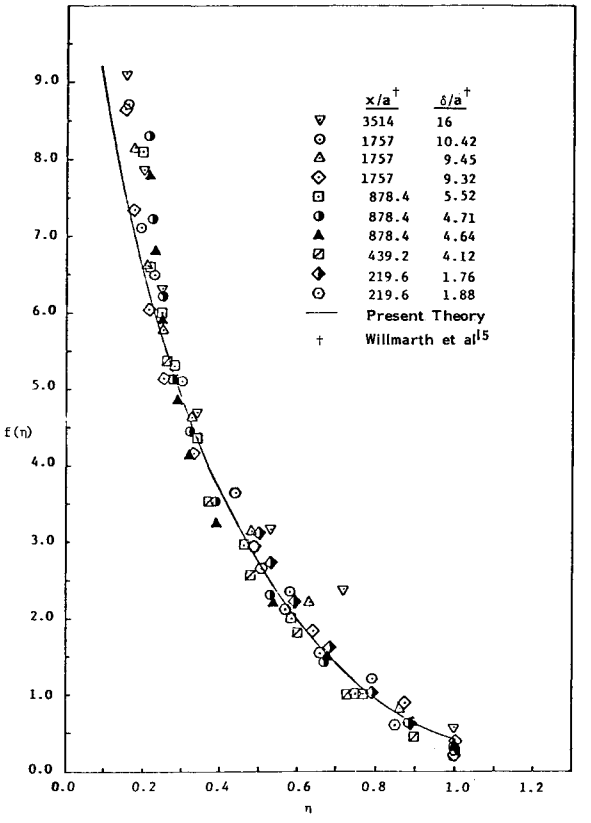

Fig. 9 Velocity-defect law.

line gave the value of B. The results are as follows:

$$R\sqrt{1-\frac{2}{R^2}} = 18.5\left(\frac{x/a}{Re_a}\right)^{5/13} \tag{76}$$

$$\frac{U_e-u}{U_e} = 4\sqrt{\frac{a}{x}}\left(1-\frac{2}{R^2}\right)^{0.65} e^{-z} U(b,1,z), \quad z=\frac{\eta^2}{2\alpha^2} \tag{77}$$

$$\alpha = \tfrac{1}{2}, \qquad b = 0.35$$

Comparisons with the data of Willmarth et al.[15] and Keshavan[6] are shown in Figs. 8 and 9.

Results and Discussion

G. Velocity Profiles

The law of the wall has been derived by using a logarithmic mixing length which takes into account the transverse-curvature effect. The logarithmic mixing length gives the usual log region in terms of the exponential integral of $\ell_n\sqrt{1+y/a}$, which can be approximated by a simple expression given by Eq. (30). The logarithmic region extends to larger values of y^* as a^* increases, as shown in Fig. 5. It also verifies that a^* is an important parameter for the law-of-the-wall region.

The velocity-defect law has been obtained by a treatment analogous to that for an axisymmetric wake in the outer region of the boundary layer. In order that the boundary layer

act like a wake, δa has to be large compared to unity which, in turn, is a result of the transverse-curvature effect. The limiting case, that of a flat-plate boundary layer, $(a \to \infty)$ is thus excluded from consideration. Willmarth's data[15] verify that the portion of the boundary layer that acts like a wake becomes larger as δ/a increases.

In the case of the flat-plate boundary layer, the logarithmic parts of the law of the wall and the velocity-defect law can be obtained by assuming that there is an overlapping region in which both laws are valid. For the cylinder, however, the assumptions made to obtain the solutions fail at the limits of the law of the wall and the velocity-defect law. In the law-of-the-wall region, it is assumed that the stress moment is constant. This implies that the inertia terms in the mean-flow momentum equation may be ignored. For large values of y^*, however, the inertia terms are no longer negligible. Furthermore, in the derivation of the velocity-defect law, it is assumed that Oseen's approximation is valid, and that the velocity gradient $\partial u/\partial y$ and the radial velocity v are small. On the contrary, as η becomes small, both of these assumptions fail. Hence, the overlapping of the inner and the outer laws, which requires continuity of the velocity gradient $\partial u/\partial y$ and consequently the continuity of the shear stress, which depends on the velocity gradient $\partial u/\partial y$ through phenomenological relations, does not occur. However, the velocity profiles calculated from the law of the wall and the velocity-defect law do intersect each other at an angle which decreases as Re_a increases. Figures 10-12 compare the velocity profiles calculated from theory with the Willmarth[15] data. As can be seen from these plots, the agreement is quite good except near the intersection point. Willmarth's data show that the intersection occurs at about $y/(\delta+a)=0.125$. For all practical purposes, the velocity profiles can be predicted using the law of the wall and the velocity-defect law, and should be smoothed by a French curve near the intersection point.

H. Estimation of Wall-Shear Stress

For the flat-plate boundary layer, the overlapping concept plays an important role in deriving a skin-friction law. Since there is no overlapping region for the present problem, a similar procedure for obtaining a skin-friction formula is not possible. For all practical purposes, however, the wall-shear stress can be determined from the intersection of the two laws, by an iterative procedure.

The velocity-defect law gives the velocity profile, up to the intersection point, by Eq. (77). After dividing and multiplying

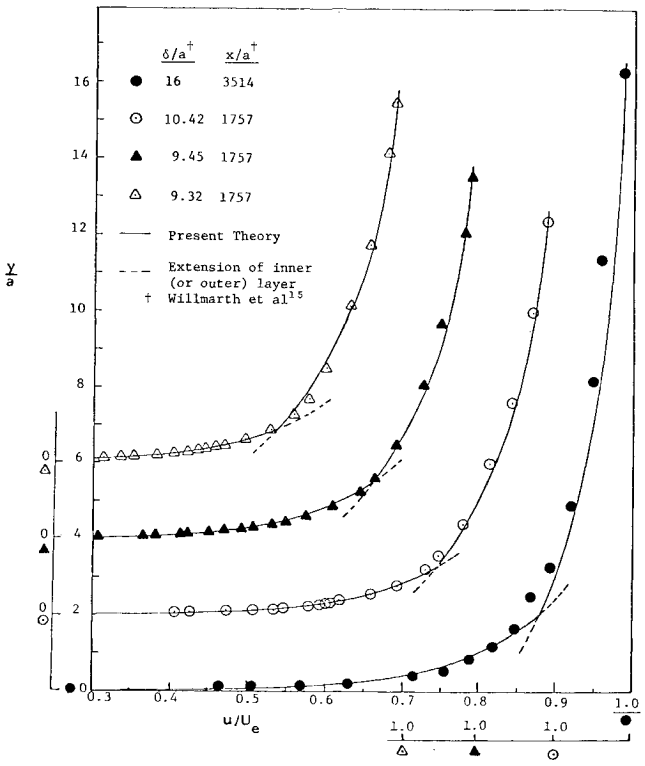

Fig. 10 Comparison of velocity profiles for $\delta/a=16$, 10.42, 9.45, 9.32.

by $\sigma = U_e/u_\tau$ at the intersection point, Eq. (77) becomes

$$\sigma - u^*(\bar{r}_c) = 4\sigma\sqrt{\frac{a}{x}}\left(1-\frac{2}{R^2}\right)^{0.65} e^{-z_c} U(b,1,z_c) \qquad (78)$$

where $z_c = 2\eta_c^2 = 2r_c^2/(\delta+a)^2$ is the point at which the two laws intersect, indicated by the subscript c. From Eqs. (27, 28b, and 29), with $a^* = Re_a/\sigma$, we have

$$u^*(\bar{r}_c) = \frac{1}{\kappa} E_i[\ln \sqrt{\bar{r}_c}] + \frac{1}{\kappa} \ln 2\frac{Re_a}{\sigma} + 5.45 - \frac{41.76}{Re_a}\sigma - \frac{\gamma}{\kappa} \qquad (79)$$

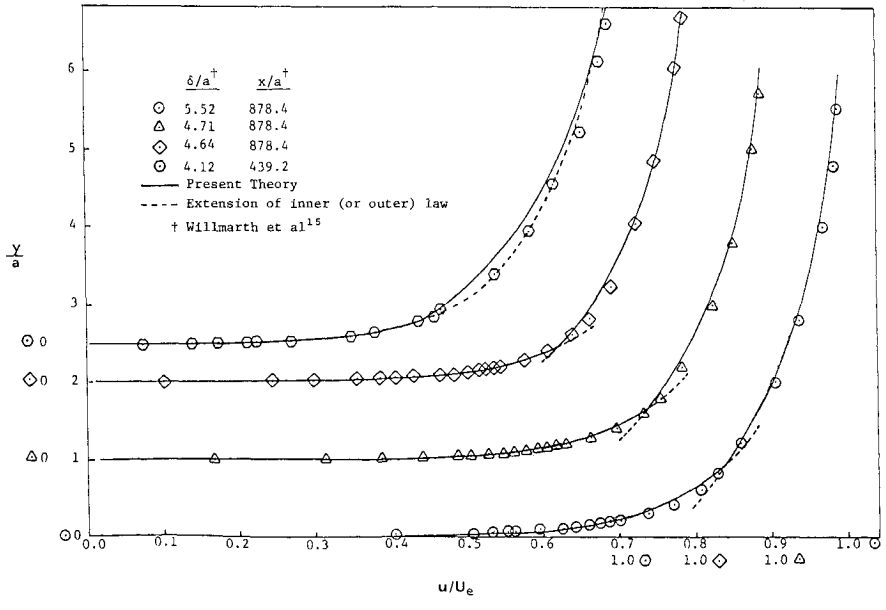

Fig. 11 Comparison of velocity profiles for $\delta/a=5.52$, 4.71, 4.64, 4.12.

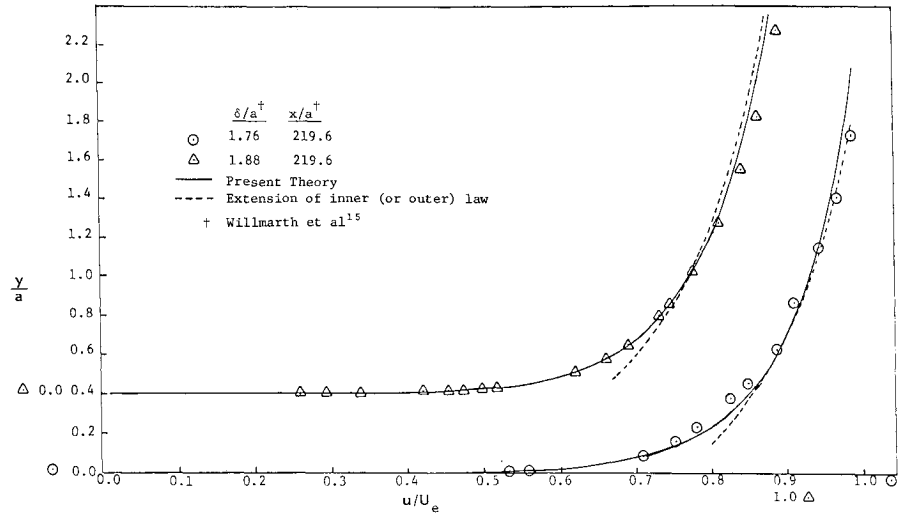

Fig. 12 Comparison of velocity profiles for $\delta/a = 1.76, 1.88$.

Table 3 Comparison of σ values

x/a	Re_a	δ/a	σ_m (Measured)	σ_c (Computed)	σ_{cp} (Clauser plot)	% Error $\left\lvert\frac{\sigma_m-\sigma_c}{\sigma_m}\right\rvert$	% Error $\left\lvert\frac{\sigma_c-\sigma_{cp}}{\sigma_{cp}}\right\rvert$
3514.0	4330	16.20	21.85	22.30	21.85	2.06	2.06
1757.0	6203	10.42	22.81	22.97	22.85	0.70	0.53
1757.0	9494	9.45	24.45	23.76	23.84	2.74	0.34
1757.0	11,693	9.32	25.61	24.26	23.62	5.27	2.71
878.4	12,790	5.52	24.91	23.98	24.08	3.73	0.42
878.4	19,230	4.71	25.60	24.41	24.30	4.65	0.45
878.4	23,100	4.64	25.92	24.82	24.27	4.25	2.27
439.2	36,680	4.12	26.96	27.30	26.65	1.26	2.44
219.6	74,260	1.76	27.41	26.02	26.21	5.07	0.72
219.6	92,310	1.88	29.23	26.99	27.26	7.66	0.99

Table 4 Comparison of displacement and momentum thickness

x/a	Re_a	δ/a	$(\delta_1/a)_d$ (Willmarth's data)	$(\delta_1/a)_c$ (Computed)	% Error in δ_1 [a]	$(\theta_1/a)_d$ (Wilmarth's data)	$(\theta_1/a)_c$ (Computed)	% Error in θ_1 [b]
3514.0	4330	16.20	6.025	5.666	5.96	5.444	5.250	3.56
1757.0	6203	10.42	3.689	3.461	6.18	3.120	3.123	0.096
1757.0	9494	9.45	2.968	2.894	2.49	2.667	2.60	2.51
1757.0	11,693	9.32	2.594	2.760	6.40	2.311	2.496	8.01
878.4	12,790	5.52	1.292	1.483	14.78	1.116	1.245	11.56
878.4	19,230	4.71	0.981	1.099	12.03	0.827	0.893	7.98
878.4	23,100	4.64	0.976	1.051	7.68	0.806	0.855	6.08
439.2	36,680	4.12	0.952	1.166	22.48	0.793	0.986	24.34
219.6	74,260	1.76	0.315	0.332	5.40	0.265	0.1884	28.91
219.6	92,310	1.88	0.337	0.375	11.28	0.261	0.238	8.81

[a] $\left\lvert\frac{(\delta_1)_d-(\delta_1)_c}{(\delta_1)_d}\right\rvert$ [b] $\left\lvert\frac{(\theta_1)_d-(\theta_1)_c}{(\theta_1)_d}\right\rvert$

Substituting Eq. (79) into Eq. (78) and rearranging gives

$$\sigma H + \frac{1}{\kappa}\ln\sigma = P \tag{80}$$

where

$$H = 1 + \frac{41.76}{Re_a} - 4\sqrt{\frac{a}{x}}\left(1-\frac{2}{R^2}\right)^{0.65} e^{-z_c} U(b,1,z_c) \tag{81}$$

$$P = 5.45 + \frac{1}{\kappa}\{E_i[\ln\sqrt{\bar{r}_c}] + \ln 2Re_a - \gamma\} \tag{82}$$

Given the values of x/a and Re_a, $R = (\delta + a)/a$ can be computed from Eq. (76) and, consequently, z_c, $\bar{r}_c$, H, and P. Therefore, σ can be computed by the iteration formula

$$\sigma_i = \frac{1}{H}\left(P - \frac{1}{\kappa}\ln\sigma_{i-1}\right) \tag{83}$$

Table 3 compares the results computed by using the above procedure with Willmarth's measured values, and the values of σ obtained from a Clauser plot.

I. Displacement and Momentum Thickness

For a thick, axisymmetric boundary layer, the displacement

and momentum thicknesses are respectively defined by[20]

$$(\delta^* + a)^2 - a^2 = \int_a^{a+\delta} \left(1 - \frac{u}{U_e}\right) d(r^2) = 2\delta_1 a \qquad (84)$$

$$(\theta + a)^2 - a^2 = \int_a^{a+\delta} \frac{u}{U_e}\left(1 - \frac{u}{U_e}\right) d(r^2) = 2\theta_1 a \qquad (85)$$

If $\bar{r}_c$ is the intersection point where the law of the wall and the velocity-defect law intersect, then Eqs. (84) and (85) can be split into two integrals to be evaluated accordingly, by using an appropriate numerical technique.[19]

Table 4 compares the displacement and momentum thicknesses computed with Willmarth's data.[15] The agreement is seen to be good, except for the last three conditions. A possible explanation for the discrepancy for these conditions is that the flow was not axisymmetric for these cases, as was indicated by Willmarth et al.[15]

Conclusions

1) For a thick, axisymmetric, turbulent boundary layer on a circular cylinder, forms of two similarity laws, one a law of the wall, the other a velocity-defect law, have been derived.

2) In the region of the law of the wall, the logarithmic mixing length is a better approximation than the linear one for the Reynolds stresses for thick, axisymmetric turbulent flows. With this logarithmic mixing length, the mean-velocity distribution, expressed as an integral, Eq. (25), or by an approximation to it which yields a logarithmic law in terms of the exponential integral, Eqs. (28a and 30), shows excellent agreement with the data. Equation (30) is recommended as a simple, analytical representation of the law of the wall for thick, axisymmetric, turbulent boundary layers.

3) The frictional Reynolds number based on cylinder radius, a^*, is an important parameter in the law-of-the-wall region. For large values of a^*, the law of the wall approaches the classical two-dimensional form.

4) Even for the intermediate values of a^*, in the region where $y^*/a^* \leq 1$, the argument of the logarithmic law $Y^* = a^*\sqrt{1 + y^*/a^*}\ \ell n(1 + y^*/a^*)$ behaves like y^*. Therefore, the Preston-tube technique can be used to measure the wall-shear stress in a thick boundary layer, with the usual calibration curve, as was assumed by Willmarth et al.[15]

5) The axial length scale, $\xi^2 = (x/a)/Re_a$, of the thick, axisymmetric, laminar boundary layer is also a proper scale for correlating a thick, turbulent boundary layer. With this scale, the boundary-layer thickness is well correlated as a power law for a wide range of values δ/a, x/a, and Re_a.

6) A velocity-defect law, in separable form $\bar{u}_d = \chi(\xi) f(\eta)$, has been obtained. This similarity assumption yields the nondimensional velocity defect, $\bar{u}_d = CR^{2(1-b)} f(\eta)$. This result shows that the velocity-defect profiles depend strongly on δ/a, as indicated by Willmarth et al.[15] The velocity-defect parameter b is a measure of the deviation from the law for an axisymmetric wake.

7) The wake portion of the boundary layer increases as δ/a becomes larger, and the wall region decreases correspondingly. Approximately ⅛th of the boundary layer obeys the law of the wall.

8) The two similarity laws do not overlap. However, they intersect at about $y/(\delta + a) = 0.125$. Boundary-layer characteristics computed by using this intersection point agree with the data within an acceptable range of error.

9) There are insufficient data, at large values of δ/a, for a variety of situations, to verify the accuracy of the velocity-defect law. As stated by Willmarth et al.,[15]

> ". . . In the future we may gain enough knowledge of the effects of transverse curvature to consider the possibility of creating an empirical formulation for the mean flow in an axisymmetric boundary layer. This was only possible in the two-dimensional case after sufficient data and understanding had accumulated, . . ."

In the present work, such a formulation has been proposed, but, in view of the paucity of the available data, it may be necessary in the future to modify the values of the constants when additional data become available.

Acknowledgment

This work was supported in part by the General Hydromechanics Research Program of the David Taylor Naval Ship Research and Development Center, under contract N00014-75-C-0273-0002, and by the Office of Naval Research, under Contract N00014-75-C-0012.

References

[1] Landweber, L., "Effect of Transverse Curvature on Frictional Resistance," David Taylor Model Basin Report No. 689, 1949.

[2] Richmond, R., "Experimental Investigation of Thick Axially Symmetric Boundary Layers on Cylinder at Subsonic and Hypersonic Speeds," Ph.D. thesis, California Institute of Technology, Pasadena, Calif., 1957.

[3] Rao, G. N. V., "The Law of the Wall in a Thick Axisymmetric Turbulent Boundary Layer," *Journal of Basic Engineering, Transactions of the ASME*, Series D. Vol. 89, March 1957, pp. 237-238.

[4] Yu, Y.S., "Effects of Transverse Curvature on Turbulent Boundary-Layer Characteristics," *Journal of Ship Research*, Vol. 3, 1959, p. 33.

[5] Chin, Y. T., Hulesbos, J., and Hunnicutt, G. H., "Effect of Lateral Curvature on the Characteristics and Skin Friction on a Turbulent Air Boundary Layer, With or Without Helium Addition," *Proceedings of the Heat Transfer and Fluid Mechanics Institute*, 1967.

[6] Rao, G. N. V., and Keshavan, N. R., "Axisymmetric Turbulent Boundary Layers in Zero Pressure Gradient Flows," *Journal of Applied Mechanics, Transactions of the ASME*, Vol. 94, 1972, p. 25.

[7] Sparrow, E. M., Eckert, E. R. G., and Minkowycz, W. J., "Heat Transfer and Skin Friction for Turbulent Boundary – Layer Flow Longitudinal to a Circular Cylinder," *Journal of Applied Mechanics*, Vol. 30, March 1963, p. 37.

[8] Patel, V. C., "A Unified View of the Law of the Wall Using Mixing-Length Theory," Iowa Institute of Hydraulic Research, Report No. 137, 1972.

[9] Landweber, L. and Poreh, M., "Frictional Resistance of Flat Plates in Dilute Polymer Solutions," *Journal of Ship Research*, Vol. 17, No. 4, 1973, pp. 227-240.

[10] White, F. M., "An Analysis of Axisymmetric Turbulent Flow Past a Long Cylinder," *Journal of Basic Engineering, Transactions of the ASME*. Vol. 94, 1972, p. 200.

[11] Cebeci, T., "Laminar and Turbulent Incompressible Boundary Layers on Slender Bodies of Revolution in Axial Flow," *Journal of Basic Engineering, Transactions of the ASME*, Series D, Vol. 92, p. 545.

[12] Afzal, N. and Narasimha, R., "Axisymmetric Turbulent Boundary Layer Along a Circular Cylinder at Constant Pressure," *Journal of Fluid Mechanics*, Vol. 74, March 1976, p. 113.

[13] Yasuhara, M., "Experiments of Axisymmetric Boundary Layers Along a Cylinder in Incompressible Flow," *Transactions of the Japan Society of Aerospace Sciences*, Vol. 2, 1959, p. 33.

[14] Willmarth, W. W. and Yang, C. S., "Wall-Pressure Fluctuations Beneath Turbulent Boundary Layers on a Flat Plate and a Cylinder," *Journal of Fluid Mechanics*, Vol. 41, p. 47.

[15] Willmarth, W. W., Winkel, R. E., Bogar, T. J., and Sharma, L. K., "Axially Symmetric Turbulent Boundary Layers on Cylinders: Mean-Velocity Profiles and Wall-Pressure Fluctuations," The University of Michigan, Department of Aerospace Engineering Gas Dynamics Laboratories, 1975.

[16] Afzal, N. and Singh, K. P., "Measurements in an Axisymmetric Turbulent Boundary Layer Along a Circular Cylinder," *Aeronautical Quarterly*, Vol. 27, 1976, p. 217.

[17] Abramowitz, M. and Stegun, I. A., *Handbook of Mathematical Functions*, Dover Publications, Inc., New York, 1970.

[18] Glauert, M. B. and Lighthill, M. J. "The Axisymmetric Boundary Layer on a Long Thin Cylinder," *Proceedings of the Royal Society*, Vol. 230, London, 1955.

[19] Denli, N., "An Analytical Solution of the Thick Axisymmetric Turbulent Boundary Layer on a Long Cylinder of Constant Radius," Iowa Institute of Hydraulic Reaserch, Ph.D. thesis, 1978.

[20] Kelly, H. R., "A Note on the Laminar Boundary Layer on a Circular Cylinder in Axial Incompressible Flow," *Journal of Aeronautical Sciences*, Vol. 21, September 1954.